Molecular Aggregation and Luminescence Behavior of Bulk Poly(2,5,2′,5′-tetrahexyloxy-8,7′-dicyano-di-*p*-phenylenevinylene)

S. H. Chen, C. H. Su, and A. C. Su*

Institute of Materials Science and Engineering, National Sun Yat-Sen University, Kaohsiung 804, Taiwan

S. A. Chen

Department of Chemical Engineering, National Tsing Hua University, Hsinchu 300, Taiwan

Received: March 12, 2004

Structural evolution and its effect on the optical absorption/emission behavior of poly(2,5,2′,5′-tetrahexyloxy-8,7′-dicyano-di-*p*-phenylenevinylene) (DH-CNPPV) upon short-term isothermal heat treatment at elevated temperatures were studied by means of a combination of X-ray diffraction, transmission electron microscopy, UV−vis spectroscopy, and photoluminescence spectroscopy. Results indicated kinetic preference for mesomorphic order in bulk DH-CNPPV, with the isotropization temperature (T_i) located in the vicinity of 210 °C. Upon heat treatment at elevated temperatures (T_a) below T_i, supramolecular self-assembly of DH-CNPPV chains results in lamellar structure ca. 2.0 nm in layer spacing. This lamellar phase exists in the form of nanodomains (ca. 10−20 nm in diameter) that agglomerate into wormlike features with DH-CNPPV backbones and the mesomorphic lamellae lying transverse to the worm's long axis. Details in the selected-area electron diffraction pattern of shear-oriented specimens prescribe a short intraboard spacing of 0.38 nm and longitudinal displacement by one-third of the repeating unit between neighboring backbones, such that adequate interaction between the cyano group and the phenylene ring is allowed for. Accompanying the thermally induced morphological changes, UV−vis light absorption behavior varies consistently with improvement or disruption of the lamellar order whereas the major emission in the photoexcited spectrum shifts from 590 to 640 nm upon emergence of mesomorphic order, which is directly excitable and hence attributable to either extended backbone conjugation or enhanced interchain delocalization in the mesomorphic state. This is in dramatic contrast to the closely related case of poly(2,5-di-*n*-octyl-oxy-1,4-phenylenevinylene) (DO-PPV) without cyano substitutions in the backbone (for which excimer emission is the preferred mode upon morphological aggregation), signifying the role of specific cyano−phenylene interaction in the ground state of aggregated chains in the mesomorphic phase.

Introduction

Poly[2-methoxy-5-(2′-ethylhexyloxy)-1,4-phenylenevinylene] (MEH-PPV) is one of the most extensively studied (and has become the 'fruit fly' of) electroluminescent polymers.[1] The concept behind the molecular design of MEH-PPV is the use of asymmetric substitutions of methyloxyl and *branched* ethylhexyloxyl side chains to improve solubility in common solvents and suppress molecular aggregation.[2] Nevertheless, there still exists a significant tendency toward molecular aggregation, which in turn gives rise to strong morphological effects on its light emission properties.[3−10] By means of X-ray diffraction (XRD) and transmission electron microscopy (TEM), we have shown for MEH-PPV the presence of molecular aggregation via formation of a biaxial nematic mesophase of sanidic nature, which is accompanied by a clear red shift of the emission maximum from 590 to 640 nm.[11,12] The 590 nm emission is attributed to single-chromophore excitons, whereas the 640 nm emission is related to molecular aggregation that may give rise to single chromophores of extended conjugation length as well as a combination of possible interchromophore mechanisms of excimers (with electronic delocalization and hence attractive intermolecular interaction in the excited-state only, dissociative in the ground state) and 'aggregates' (with electronic delocalization and hence attractive intermolecular interaction in both the excited and the ground states).[13]

One possible explanation for the observed molecular aggregation is that the methoxyl substituent is too short to provide adequate shielding of the backbone to avoid interbackbone contacts in MEH-PPV. This is based on the idea that the formation of aggregates is driven mainly by the aromatic−aromatic attraction between backbones. On the other hand, as previously proposed for hairy-rod polymers in general, molecular aggregation may simply be a result of incompatibility between the flexible (aliphatic) side chains and the semirigid (aromatic) backbones, reminiscent of comb-shaped block copolymers and side-chain liquid crystalline polymers.[14] In better agreement with this latter expectation, Fann et al.[15−18] previously proposed that significant intermolecular aggregation occurs in the case of poly(2,5-di-*n*-octyloxy-1,4-phenylenevinylene) (DO-PPV), a close homologue of MEH-PPV but with comparatively long and linear side-chain substitutions. More recently, our morphological study[19] of bulk DO-PPV has shown that molecular aggregation indeed occurs in DO-PPV via formation of a lamellar mesophase, in support of the idea that it is generally the amphiphilicity (van der Waals interactions between aliphatic side chains and those between aromatic backbones) that is responsible for the observed supramolecular self-assembly. In this case, the formation of the mesomorphic order also bears significant effects on optical absorption and emission properties

* To whom correspondence should be addressed. E-mail: acsu@mail.nsysu.edu.tw.

10.1021/jp0488923 CCC: $27.50
Published on Web 05/29/2004

in terms of competition between single-chromophore and excimer-like emissions at 590 and 630 nm, respectively.

As an extension of previous studies, here we present our recent observations over poly(2,5,2′,5′-tetra-*n*-hexyloxy-8,7′-dicyano-di-*p*-phenylenevinylene) (DH-CNPPV) that bears symmetrically attached linear alkoxyl side chains as well as polar cyano substitutions on the main chain, hence of enhanced interbackbone attraction. This polymer was first considered as one of the candidate materials for electron-transport layers due to its high electron affinity (as endowed by the cyano functionality) but was later found to emit red light.[20] Rather extensive studies[21−28] on its photophysical properties in films as well as in solutions have subsequently been made, and it is generally agreed that the red-light emission is originated from interchain species. However, no general consensus has been reached regarding the exact photophysical entities involved. More recent low-temperature results[29] indicated a similar photoluminescence spectral width at 10 K and room temperature, indicating a broad distribution of states (rather than thermal broadening) and hence implying inherent heterogeneity in the dip-cast film. This is consistent with a pioneering morphological study[30] of DH-CNPPV films in which formation of an ordered structure (described as 'crystalline') was suggested on the basis of observations from differential scanning calorimetric (DSC) and X-ray diffraction (XRD) analysis. However, in view of our recent results on MEH-PPV and DO-PPV, the presence of a mesomorphic phase appears to be a distinct possibility that should be considered.

In this follow-up study, we present more detailed analysis via microscopic as well as diffraction techniques to show that this ordered phase should more appropriately be described as a mesomorphic lamellar phase. Consistent with the stronger interbackbone attraction, this mesophase is comparatively better ordered in terms of intraboard backbone stacking than the corresponding mesophases of MEH-PPV and DO-PPV and yet bears similar morphological features of locally aligned nanodomains; also identified is its characteristic emission at 640 nm that is directly excitable and hence should originate from single chromophores of extended conjugation length or interchain 'aggregate' emission.

Experimental Section

Synthesis and characterization of the DH-CNPPV sample (with weight-average molecular mass M_w = 45 kDa and polydispersity index PDI = 2.5, chemical structure given as inset in Figure 1b) used in this work have been previously reported in detail.[30] The as-synthesized sample was then carefully stored in the dark in an argon-flushed vessel. Similar protective measures were adopted for all film specimens prepared.

Differential scanning calorimetric (DSC) measurements were made by use of a TA Q100 instrument routinely calibrated using indium and lead standards and operated under a stream of nitrogen gas. Polarized light microscopic (PLM) observations were made by use of a Nikon Eclipse E400-POL microscope equipped with a nitrogen-protected heating stage (Linkam THMS-600) and a temperature controller (Linkam TMS-91). A Siemens D5000 diffractometer equipped with a copper target (Kα line, with wavelength $\lambda = 0.154$ nm), a graphite collimator, and a standard sample holder was used to obtain 1-D ('powder') X-ray diffraction (XRD) profiles at room temperature under a step−scan rate of 0.05° per 2 s in the scattering angle range of $2\theta = 1^{-}41°$ unless specified otherwise. Transmission electron microscopic (TEM) studies were performed using a JEOL 3010 instrument under an acceleration voltage of 200 kV, at which the combined factor of wavelength and camera length has been carefully calibrated using (111), (200), (220), and (311) reflections from vapor-deposited Al thin film. Surface topographic features were examined via secondary electron images obtained by use of a field-emission scanning electron microscope (JEOL JSM-6330TF) under an accelerating voltage of 10 kV. Optical absorption (UV−vis) and photoluminescence (PL) spectra of the film specimens were obtained by use of a Hong-Ming MFS-230 instrument.

Solutions of DH-CNPPV in toluene (ca. 0.1% for TEM specimens and 0.2% for all other specimens) prepared by

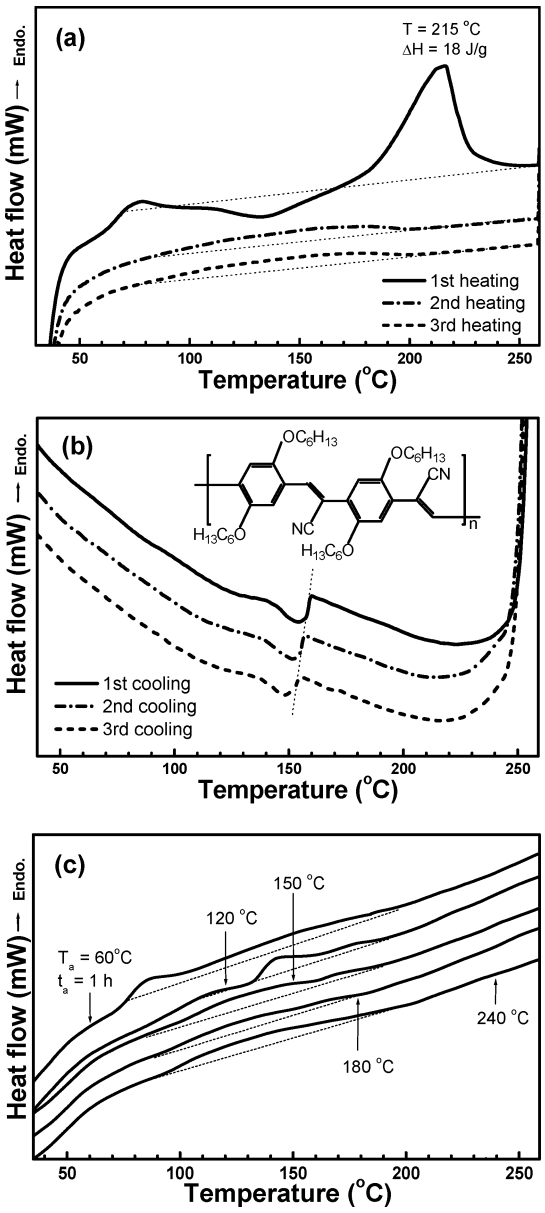

Figure 1. DSC thermograms of bulk DH-CNPPV during three consecutive cycles (with heating or cooling rate of 20 °C/min) between 30 and 260 °C: (a) heating and (b) cooling traces. Note that the original melting at 215 °C never recovers in the later cycles. The exotherm in the vicinity of 150 °C during cooling shifted to slightly lower temperatures with repeated heating, indicating increased supercooling required for nucleation of the ordered phase that corresponds to the weak and broad endotherm between 80 and 210 °C in the subsequent heating trace. (c) Heating traces right after 1-h isothermal treatment at a selected annealing temperature (T_a, ranging from 60 to 240 °C) and subsequent fast cooling to room temperature, showing clear reorganization effects for $T_a \leq 180$ °C.

warming in a hot water bath up to 80−90 °C were used for drop casting of film specimens on quartz or glass substrates. Oriented TEM specimens were prepared via manual shearing (by sweeping a blade over the solution-cast film) at an elevated temperature (180 or 220 °C), followed by fast cooling to room temperature. In the case of shearing at 220 °C, an additional annealing procedure (5 min at 180 °C after shear) was adopted to allow for better development of mesomorphic structure. These specimens were then floated off the substrate using 1% aqueous HF solutions, washed in deionized water, vacuum-dried, followed by evaporation coating with carbon or sometimes a combination of Pt/C under vacuum. We note that the use of dilute HF solutions is to chemically etch the surface of the glass substrate; the detachment is easily achieved in seconds. This procedure has been successfully applied to quite a number of polymers in this laboratory without adverse effects in morphological characteristics of the thin films prepared.

Results and Discussion

Thermal Behavior. Given in Figure 1 are DSC thermograms of *as-synthesized* DH-CNPPV (after long-term room-temperature storage) upon repeated cycling between room temperature and 260 °C at fixed heating or cooling rates of 20 °C/min. During the first heating there is a broad exotherm between 80 and 160 °C, followed by a prominent endotherm (with an enthalpy of transition $\Delta H = 18$ J/g comparable to a previous result[30] of 15 J/g) in the vicinity of 215 °C (previously observed at 210 °C) attributable to the melting of a crystalline phase as previously assigned. During the subsequent cooling scan (not recorded in the previous study) there exists an exotherm (with a low-temperature tail) below 160 °C (i.e., more than 50 °C in supercooling), signifying the formation of an ordered phase that is nucleation-controlled and hence of significant positional order. This ordered phase, however, is *not* the crystalline phase, as indicated by clear differences in XRD profiles (presented in following paragraphs) and the fact that the prominent melting peak does not reappear in the subsequent heating trace. Instead, a weak and broad endotherm encompassing the temperature range of 80−200 °C (which was left unnoticed in the earlier work) is identified in the second heating. Both the cooling exotherm and the broad heating endotherm are repeatedly reproducible in later scans.

The broad endotherm is similar to that[12] observed in the case of MEH-PPV, which has been attributed to the gradual dissipation of mesomorphic order upon heating. On the other hand, as shown in Figure 1c, isothermal heat treatment of DH-CNPPV at an annealing temperature (T_a) between 60 and 150 °C resulted in an extra endothermic contribution located ca. 20 °C *above* the corresponding T_a. This is consistent with the assignment of a mesomorphic phase with *some* positional order, as structural perfection upon isothermal annealing is generally observed for systems with positional order. We note that no such perfection effect exists in the case of MEH-PPV, for which a biaxial nematic phase of only orientational order has been assigned.

The assignment of a mesophase upon cooling from the melt is also supported by PLM observations on a *solution-cast* specimen, as given in Figure 2, where micrographs were taken during the second cycle between room temperature and 210 °C. The optical features were rather weak in the *as-cast* film and showed little information (except for a preliminary identification of isotropization temperature T_i in the vicinity of 200 °C) in the first cycle. Clear crystalline features were not observed for the as-cast films, indicating significant differences between the

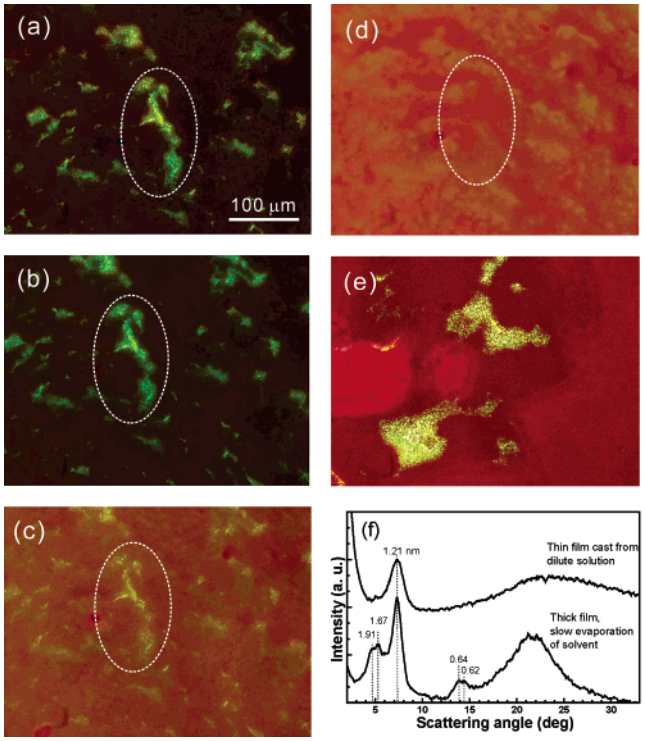

Figure 2. PLM micrographs of drop-cast specimen of DH-CNPPV over a fixed region during thermal cycling (with heating or cooling rate of 20 °C/min) between room temperature and $T_i = 210$ °C: (a) 30 °C, (b) 180 °C, and (c) 190 °C during heating, and (d) 40 °C during cooling; the nematic-like optical texture was only weakly recovered upon cooling to room temperature. Regions that were originally isotropic, however, may become anisotropic with emerging nematic texture during cooling as shown in e, where the micrograph was taken at a different region after cooling to room temperature. The XRD profiles in f demonstrate development of significant crystalline order upon slow solvent removal by allowing the solution to dry gradually in a beaker over a period of several days.

as-synthesized bulk state and *as-cast* films (with accelerated residual solvent removal in a vacuum). This is consistent with the XRD profile of the as-cast film (upper curve, Figure 2f), where only a broad peak located around $2\theta = 7°$ (ca. 1.2 nm in *d* spacing) is discernible over a generally featureless background. Nevertheless, crystalline features do appear in thicker films cast from more concentrated solution upon slow solvent removal (lower curve, Figure 2f), consistent with the assignment of a melting peak around 215 °C in the first heating trace in Figure 1a. The presence of such a solvent-induced crystalline phase in *as-synthesized* DH-CNPPV may probably be traced back to the final purification step (precipitation into methanol followed by prolong stirring before filtering and vacuum drying) in the synthesis procedure.[30] In the following, we focus on observations made during the second heating/cooling cycle, in which transformation involving a crystalline phase is safely excluded on the basis of DSC results.

Figure 2a shows the limited development of nematic-like optical texture after cooling from the isotropic melt, in which the anisotropic regions dimmed in the second heating as T_i is approached (Figure 2b,c) and did not quite recover upon cooling (Figure 2d). Interestingly, regions that had appeared nearly isotropic became more distinctively birefringent (Figure 2a−e), indicating self-assembling of disordered chains into mesomorphic order. The more efficient reorganization of the originally disordered region during cooling, in contrast to difficulties in structural recovery in regions of freshly dissipated order, indicates clear path dependence in the ordering of DH-

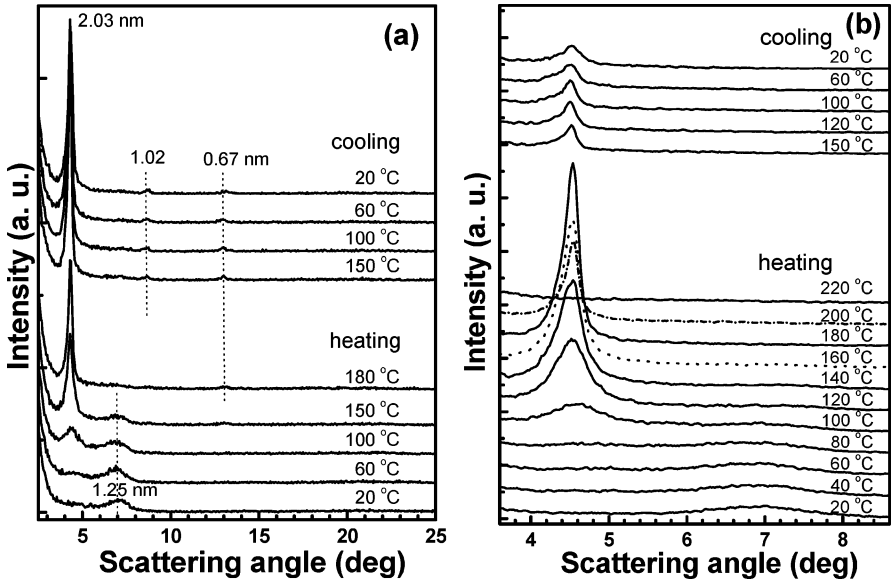

Figure 3. High-temperature XRD profiles of drop-cast DH-CNPPV films in a sequence (bottom to top) of isothermal measurements in which the temperature was stepwise increased from 20 °C to (a) 180 °C ($2\theta = 1°$ to 41°, at a step scan rate of 0.05°/2 s, and each profile took approximately 27 min) or (b) 220 °C, at a step scan rate of 0.02°/2 s (each profile took approximately 8.5 min), then stepwise decreased to room temperature.

CNPPV that is commonly observed in *far-from-equilibrium* processes. These features are repeatedly observed in subsequent cycles for ensured reproducibility.

Structural Development. Given in Figure 3a are high-temperature XRD profiles obtained during a temperature cycle between 20 and 180 °C. As discussed in the last subsection, the weak maximum near $2\theta = 7°$ for the *as-cast* film at 20 °C indicates some poorly developed crystalline order during film formation. This peak, however, weakened when the temperature was stepwise increased to 150 °C and disappeared upon a further increase of temperature to 180 °C. Meanwhile, the reflection located near $2\theta = 4.5°$ (corresponding to a *d* spacing value of 2.0 nm) emerged as the temperature is increased to 100 °C, and its intensity increased with increasing temperature up to 180 °C. The XRD profiles taken during the subsequent cooling steps indicate further structural perfection, resulting in clearly identifiable second- and third-order reflections attributable to a mesomorphic phase with lamellar order.

Given in Figure 3b are profiles taken in another series of high-temperature XRD measurements on a separate freshly cast specimen, in which a narrower 2θ range was adopted to emphasize the lower angle region as the temperature was cycled between 20 and 220 °C to explore the effect of heating above T_i. The mesomorphic order, developed between 100 and 180 °C, became weakened at 200 °C and fully dissipated at 220 °C, indicating $T_i \approx 210$ °C as suggested by PLM observations. More interestingly, heating above T_i resulted in only partial recovery of mesomorphic order upon subsequent cooling, implying retarded transformation. This retardation effect upon cooling above T_i, however, is not as strong as in previous cases[12,19] of MEH-PPV and DO-PPV, as partially recovered structural order may still be identified in the room-temperature XRD profiles (shown in Figure 4) of fast-cooled films in a sequence of short-term (i.e., 5 min) heat treatments at stepwise increased annealing temperature (T_a) up to 220 °C.

Morphological Features. Given in Figure 5a is a representative bright-field image of specimens after a typical 5-min heat treatment at 180 °C, showing development of domains approximately 10−20 nm in size. Mechanical shearing at an elevated temperature resulted in less well developed domains (cf. Figure 5b), but an additional 5-min heat treatment at 180 °C *after* shear restores the nanodomain morphology and, in addition, shows that these nanodomains tend to array into stripes transverse to the shear direction, similar to earlier observations[12,19] on MEH-PPV and DO-PPV specimens. Confirmation of the nanodomain morphology is provided by secondary electron images in Figure 5d,e in which surface topological features of similarly processed (albeit thicker) specimens are demonstrated. The presence of interdomain cracks developed upon electron beam bombardment signifies weak interdomain adhesion. These features are similar to corresponding observations in our previous studies[12,19] of MEH-PPV and DO-PPV, which have been interpreted in terms of collapse of single (or a very small number of) chains upon solvent evaporation during film formation.[12]

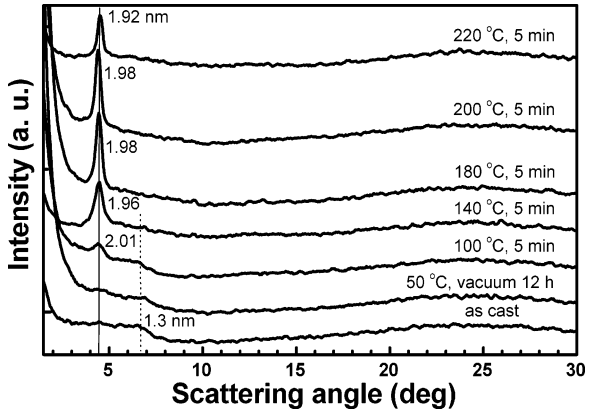

Figure 4. Room-temperature XRD profiles of drop-cast DH-CNPPV specimen upon fast cooling to room temperature during a sequence of 5-min heat treatments at stepwise increased T_a. The residual order in the case of $T_a = 220$ °C is attributed to improved structural order during the sequence of heat treatments and prompt recovery during cooling due to memory effects.

Molecular Packing. Given in Figure 6 are representative selected-area electron diffraction (SAED) patterns of sheared DH-CNPPV specimens. The lamellar structure is clearly demonstrated by equatorial arcs (up to third order) in Figure 6a, signifying layered structure with interlayer spacing of 2.0 nm. In view of the tendency toward segregation between semirigid backbones and flexible side chains, the lamellar

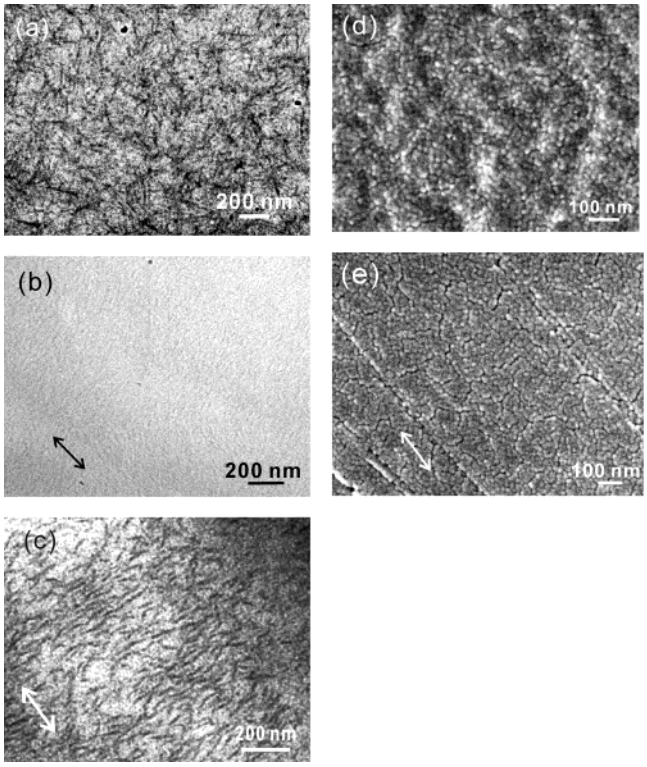

Figure 5. TEM bright field images of specimens (a) annealed for 5 min at 180 °C, (b) sheared at 180 °C, and (c) sheared at 200 °C and subsequently annealed for 5 min at 180 °C, followed by fast cooling to room temperature; FE-SEM micrographs of films prepared in a manner similar to a and b are given as d and e, respectively. The direction of shear is indicated by two-way arrows in b and c and groves in e.

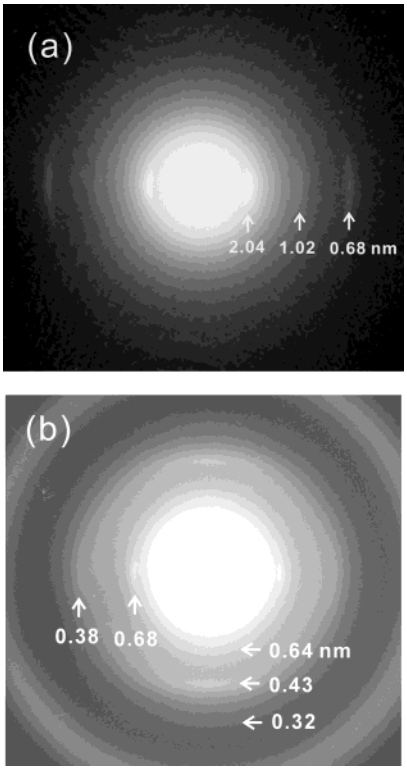

Figure 6. Selected-area electron diffraction patterns (taken at different camera lengths) of shear-oriented specimens (shear direction parallel to the meridian) showing (a) sharp equatorial arcs corresponding to layer spacing of 2.04 nm and (b) an additional equatorial arc signifying an interbackbone spacing of 0.38 nm. Meridional arcs with *d* spacing values of 0.64 and 0.32 nm correspond to one-half of a repeating unit, suggesting 2_1-screw symmetry along the backbone. The 'extra' meridional reflection (0.43 nm in *d* spacing) is stronger and broader than the other meridional arcs and hence attributed to relative displacement of one-third repeat length between neighboring DH-CNPPV chains to facilitate interbackbone attraction through cyano groups. The outer ring (ca. 0.2 nm in *d* spacing) corresponds to the 'amorphous' halo of vacuum-deposited Pt.

structure is most likely composed of boards of stacked semirigid backbones separated by regions rich in aliphatic side chains, as in similar cases of DO-PPV and MEH-PPV. In Figure 6b (taken at a longer camera length), an additional equatorial reflection (ca. 0.38 nm in *d* spacing) may be observed, which is attributed to interbackbone stacking distance within the board-like lamellae. Note that this is shorter than the interbackbone stacking distance of 0.40 nm in MEH-PPV or 0.41 nm in DO-PPV, consistent with the expectedly stronger interbackbone attraction due to the presence of electron-withdrawing cyano groups in the present case.

Along the meridian, there are arcs (ca. 0.64 and 0.32 nm in *d* spacing) attributable to the monomer repeat length of 1.28 nm, which is comparable to twice the length of the phenylenevinylene unit, i.e., ca. 0.67 and 0.63 nm, of MEH-PPV and DO-PPV, respectively.[12,19] The absence of the reflection at a full repeat length of 1.28 nm suggests extinction due to the presence of 2_1-screw symmetry along the backbone. Note that this attribution is not in conflict with the presence of the meridional arc with *d* spacing of 0.43 nm (which coincides with one-third of the repeat distance), as the latter is different in shape with other meridional reflections.

Results from single-crystal X-ray analysis and quantum-mechanical calculations of oligomeric analogues of CN-DHPPV have indicated a fairly coplanar (i.e., with only slight waviness) backbone conformation and that the negatively charged (i.e., −0.15 electron unit) cyano nitrogen tends to sit right above the center of the positively charged (i.e., +0.07 electron unit) phenylene ring (at a rather short distance of 0.33 nm between N atom and center of phenylene ring) in the neighboring molecule.[31,32] We therefore propose that DH-CNPPV backbones are stacked in a manner shown schematically in Figure 7a, in which adequate interactions between cyano and phenylene groups are allowed. Note that the slightly negative ether linkage is in close contact with a vinylene carbon, in favor of further electrostatic attraction. It turns out that this model results in a longitudinal displacement between neighboring backbones by approximated one-third of a repeating unit (Figure 7b), explaining the peculiar presence of the meridional arc ca. 0.43 nm in *d* spacing.

As there are no discernible off-axis reflections, the alkyl side chains are believed to pack in a somewhat disordered manner (Figure 7c). Full extension of the *n*-hexyloxy group results in an arm length of 0.85 nm. With the backbone width of 0.5 nm and lamellar spacing of ca. 2.0 nm, this translates to an average tilt of side chains from lamellar normal by ca. 25°. Schematic presentation of the proposed lamellar structure is given in Figure 7c.

Optical Absorption/Emission. As shown in Figure 8a,b, both absorption and emission spectra are significantly affected by changes in molecular packing. The absorption spectrum is clearly red-shifted upon heat treatments up to $T_a = 200$ °C. This is followed by a blue shift after the 5-min annealing at 220 °C, consistent with the partial loss of structural order shown in Figure 4. This simple correspondence between the absorption spectrum and structural development, however, is not followed in the emission behavior. The emission spectrum (at an

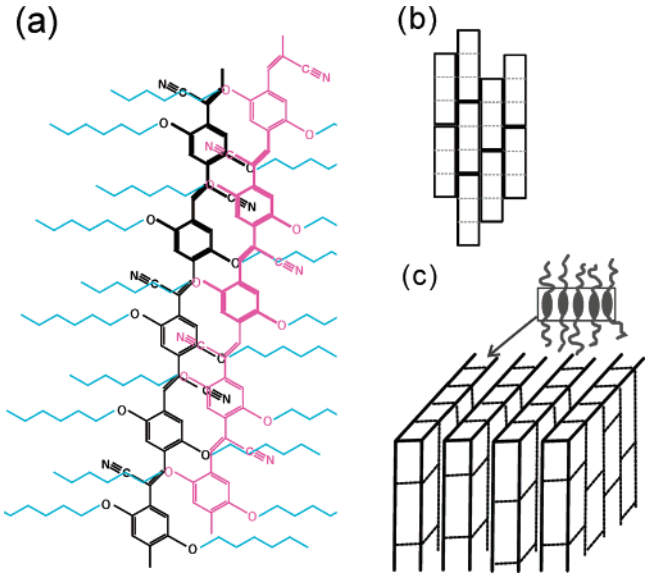

Figure 7. Schematic presentations of molecular packing in the mesomorphic structure: (a) stacking of neighboring backbones with cyano nitrogen situated in close proximity to a phenylene ring in the neighboring chain, which results in a relative displacement by one-third of a repeating unit for neighboring backbones as depicted in b; (c) resulting lamellar mesophase structure with boards of stacked backbones separated by flexible side chains.

excitation wavelength $\lambda_{ex} = 480$ nm) of the as-cast DH-CNPPV film has a main peak at ca. 600 nm and a shoulder at ca. 640 nm. The relative intensity of the former decreases and the contribution from the latter increases significantly upon heat treatments at elevated temperatures (and development of structural order), resulting in a dramatic shift of the emission maximum from ca. 600 to 640 nm. Interestingly, although the emergence of lamellar order strongly affects the emission behavior, the *extent* of the developed structural order has little effects on the emission spectrum. For example, emission spectra after heat treatments at 100−220 °C essentially fall into a single curve although there are significant differences in the *extent* of ordering as indicated by the corresponding XRD profiles in Figure 4.

The fact that the *extent* of the developed lamellar order has little effect on the emission spectrum deserves further comment. As the absorption spectrum varies clearly with the growth or the disappearance of the mesomorphic phase, it is clear that the excitation of chromophores is not responsible for the insensitivity of the emission behavior with the extent of ordering. Hence, we propose that the mesomorphic aggregates act as funnels of excitation energy via a sequence of resonance energy transfer[13] from single-chromophore excitons on disordered chains. It is well known that energy transfer may occur when the emission wavelength of the donor (i.e., the single-chain chromophores here, emitting at ca. 600 nm) overlaps with the absorption band of the acceptor (i.e., the mesomorpic aggregates here, absorbing in the vicinity of 600 nm). The action of the resonance energy transfer is most efficient within the Forster distance, typically on the order of 5 nm. In the present case of efficient quenching of single-chromophore emission with only a minor presence of lamellar order, the mesomorphic aggregates must be rather finely distributed within the disordered matrix as also implied by Figure 5.

Corresponding to Figure 8b in which $\lambda_{ex} = 480$ nm, changes in emission spectra at $\lambda_{ex} = 600$ nm are given in Figure 8c. At this long excitation wavelength the emission at 640 nm may still be excited, signifying that the emission at 640 nm is not

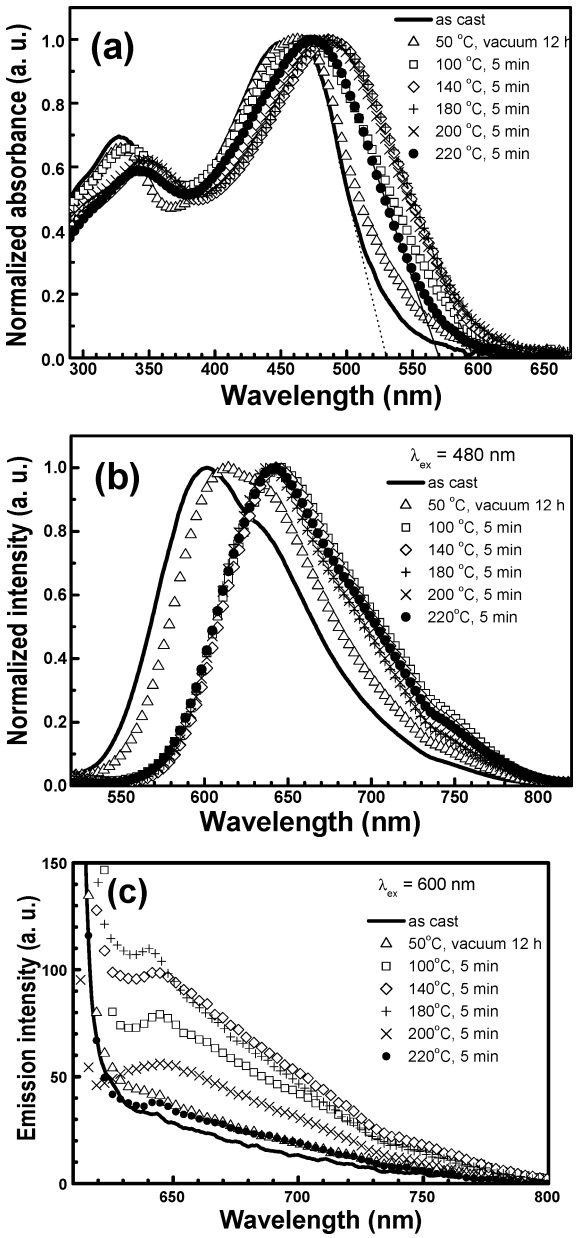

Figure 8. (a) Normalized absorption, (b) normalized emission spectra excited at $\lambda_{ex} = 480$ nm, and (c) emission spectra excited at $\lambda_{ex} = 600$ nm of drop-cast DH-CNPPV film upon fast cooling to room temperature during a sequence of 5-min heat treatments at stepwise increased T_a. Note that the thermal history here follows generally that of the XRD study in Figure 4.

excimeric in nature. In addition, the emission intensity correlates well with the development and dissipation of mesomorphic order, indicating the absence of energy funneling from high-energy species as compared to Figure 8b. All these observations indicate that the 'red' emission at 640 nm is in direct correspondence with the formation of mesomorphic order. Results of the present morphological study are consistent with the interpretation of single-chromophore excitons of extended conjugation length or that in terms of interchain 'aggregate' emission.

Conclusion

By means of detailed analysis via microscopic as well as diffraction techniques, we demonstrated the predominant formation of lamellar mesophase in DH-CNPPV films, which was incorrectly attributed as 'crystalline' in our earlier report.[30]

Consistent with the stronger interbackbone attraction, this mesophase structure bears higher positional order in terms of intraboard backbone stacking as compared to the corresponding mesophases of MEH-PPV and DO-PPV. Similarity in morphological features of locally aligned nanodomains, however, is retained. Also identified is the characteristic emission at 640 nm of the lamellar mesophase, which is directly excitable and hence should be attributable to single chromophores of extended conjugation or interchain 'aggregate' emission.

We note that this is in dramatic contrast to the closely related case of DO-PPV without cyano groups in the backbone,[19] which shows stronger tendency toward mesomorphic aggregation (attributable to stronger segregration power due to longer side chains) but resulted in *excimer* emission. This clearly indicates the significant role played by interbackbone interaction (between the cyano and the phenylene groups in the present case of DH-CNPPV) in the aggregated state. In comparison, the asymmetrically substitutions of shorter or branched side chains in the case of MEH-PPV[13] resulted in comparatively weaker tendency toward mesomorphic aggregation (as may be seen by comparing Figures 3−5 here with Figures 3−5 in ref 13 and Figures 2−5 in ref 19) and yet photoluminescence behavior intermediate to the two extreme cases of DO-PPV and DH-CNPPV. It is therefore concluded that *morphological aggregation* in these polymers is not related to photophysical processes in a straightforward manner; whether there exist specific interbackbone attractions in the ground state of the aggregated phase (such as the donor−acceptor interaction between cyano and phenylene groups in the present case of DH-CNPPV) is probably more relevant in this respect.

Acknowledgment. We gratefully acknowledge financial support from the Ministry of Education and the National Science Council under contract numbers 91E-FA04-2-4A and NSC91-2216-E−110-007, respectively.

References and Notes

(1) Friends, R. H.; Gymer, R. W.; Holmes, A. B.; Burroughes, J. H.; Marks, R. N.; Taliani, C.; Bradley, D. D. C.; dos Santos, D. A.; Gredas, J. L.; Loglund, M.; Salaneck, W. R. *Nature (London)* **1999**, *397*, 121.

(2) Kraft, A.; Grimsdale, A. C.; Holmes, A. B. *Angew. Chem., Int. Ed. Engl.* **1998**, *37*, 402.

(3) Nguyen, T. Q.; Doan, V.; Schwartz, B. J. *J. Chem. Phys.* **1999**, *110*, 4068.

(4) Shi, Y.; Liu, J.; Yang, Y. *J. Appl. Phys.* **2000**, *87*, 4254.

(5) Nguyen, T. Q.; Martini, I. B.; Liu, J.; Schwartz, B. J. *J. Phys. Chem. B* **2000**, *104*, 237.

(6) Lee, T. W.; Park, O. O. *Adv. Mater.* **2000**, *12*, 801.

(7) Liu, J.; Shi, Y.; Ma, L.; Yang, Y. *J. Appl. Phys.* **2001**, *88*, 605.

(8) Nguyen, T. Q.; Schwartz, B. J.; Schaller, R. D.; Johnson, J. C.; Lee, L. F.; Haber, L. H.; Saykally, R. J. *J. Phys. Chem. B* **2001**, *105*, 5153.

(9) Tan, C. T.; Inigo, A. R.; Fann, W. S.; Wei, P. K.; Perng, G. Y.; Chen, S. A. *Org. Electron.* **2002**, *3*, 81.

(10) Collison, C. J.; Rothberg, L. J.; Treemaneekarn, V.; Li, Y.*Macromolecules* **2001**, *34*, 2346.

(11) Chen, S. H.; Su, A. C.; Huang, Y. F.; Su, C. H.; Peng, G. Y.; Chen, S. A. *Macromolecules* **2002**, *35*, 4229−4232

(12) Chen, S. H.; Su, A. C.; Chou, H. L.; Peng, K. Y.; Chen, S. A. *Macromolecules* **2004**, *37*, 167.

(13) Pope, M.; Swenberg, C. E. *Electronic Processes in Organic Crystals*; Oxford University Press: New York, 1982. As '*aggregate emission*' bears a particular photophysical definition, which is more specified than *molecular aggregati*on in broader senses as is commonly used, quotation marks will be used throughout this article whenever the photophysical definition is emphasized.

(14) Watanabe, J.; Harkness, B. R.; Sone, M.; Ichimura, H. *Macromolecules* **1994**, *27*, 507.

(15) Hsu, J. H.; Fann, W.; Tsao, P. H.; Chuang, K. R.; Chen, S. A. *J. Phys. Chem. A* **1999**, *103*, 2375.

(16) Chang, R.; Hsu, J. H.; Fann, W. S.; Yu, J.; Lin, S. H.; Lee, Y. Z.; Chen, S. A. *Chem. Phys. Lett.* **2000**, *317*, 153.

(17) Hsu, J. H.; Hayashi, M.; Lin, S. H.; Fann, W.; Rothberg, L. J.; Perng, G. Y.; Chen, S. A. *J. Phys. Chem. B* **2002**, *106*, 8582.

(18) Hsu, J. H.; Chang, R.; Lin, S. H.; Fann, W.; Perng, G. Y.; Chen, S. A. *Phys. Rev. B*, submitted for publication .

(19) Chen, S. H.; Su, A. C.; Han, S. R.; Chen, S. A.; Lee, Y. Z. *Macromolecules* **2004**, *37*, 181.

(20) Greenham, N. C.; Moratti, S. C.; Bradley, D. D. C.; Friend, R. H.; Holmes, A. B. *Nature* **1993**, *365*, 6281.

(21) Oelkrug, D.; Tompert, A.; Egelhaaf, H.-J.; Hanack, M.; Steinhiber, Hohloch, M.; Meier, H.; Stalmach, U. *Synth. Met.* **1996**, *83*, 231.

(22) Baigent, D. R.; Holmes, A. B.; Moratti, S. C.; Friend, R. H. *Synth. Met.* **1996**, *80*, 119.

(23) Samuel, I. D. W.; Rumbles, G.; Collison, C. J. *Phys. Rev. B* **1995**, *52*, 11573.

(24) Harrison, N. T.; Baigent, D. R.; Samuel, I. D. W.; Friend, R. H.; Grimsdale, A. C.; Moratti, S. C.; Holmes, A. B. *Phys. Rev. B* **1996**, *53*, 15817.

(25) Conwell, E. M.; Perlstein, J.; Shaik, S. *Phys. Rev. B* **1996**, *54*, R2306.

(26) Samuel, I. D. W.; Rumbles, G.; Collinson, C. J.; Friend, R. H.; Moratti, S. C.; Holmes, A. B. *Synth. Met.* **1997**, *84*, 497.

(27) Rumbles, G.; Samuel, I. D. W.; Collinson, C. J.; Miller, P. F.; Moratti, S. C.; Holmes, A. R. *Synth. Met.* **1999**, *101*, 158.

(28) Rumbles, G.; Collison C. J.; Russell D. L.; Magnani, L. A.; Holmes, A. B.; Moratti, S. C.; Samuel, I. D. W. *Synth. Met.* **2000**, *111−112*, 501.

(29) Hsu, J. H.; Fann, W.; Meng, H. F.; Chen, E. S.; Chang, E. C.; Chen, S. A.; To, K. W. *Chem. Phys.* **2001**, *269*, 367.

(30) Chen, S. A.; Chang, E. C. *Macromolecules* **1998**, *31*, 4899.

(31) Gill, R. E.; Meetsma, A.; Hadziioannou, G. *Adv. Mater.* **1996**, *8*, 212.

(32) Gill, R. E.; van Hutten, P. F.; Meetsma, A.; Hadziioannou, G. *Chem. Mater.* **1996**, *8*, 1341.